Synthesis and Optical Properties of Doped $CsPbCl_3$ Nanocrystals

*Wencai He, Qiqi Zhang, Yifang Qi, Jaiden Moore, Paresh Ray, Nihar Pradhan, Xianchun Zhu, Fengxiang Han, Tigran Shahbazyan, and Qilin Dai**

Department of Chemistry, Physics, and Atmospheric Sciences, Jackson State University, 1400 John R. Lynch Street, Jackson, MS 39217, United States

*corresponding author: qilin.dai@jsums.edu

Keywords: $CsPbCl_3$; Optical properties; Tb; Mn; Doped

Abstract

Tb, Mn, and Br ions are introduced to $CsPbCl_3$ to prepare doped $CsPbCl_3$ nanocrystals by hot injection method. The prepared doped $CsPbCl_3$ nanocrystals are characterized by x-ray diffraction (XRD), transmission electron microscopy (TEM), and photoluminescence (PL) techniques to study the structural, morphological, and optical properties. The structure is not influenced by doping, which is confirmed by XRD data. Tb doping leads to larger particle sizes compared to undoped $CsPbCl_3$ nanocrystals (8 nm ➔12 nm). However, the Mn and Br doping doesn't affect the sizes that much. The optical properties of $CsPbCl_3$ nanocrystals can be controlled by doping. Green emission at 543 nm from Tb is observed for $CsPbCl_3$:Tb nanocrystals. Red emission at 590 nm is obtained for Mn doping. Controlled exciton emission from $CsPbCl_3$ is achieved by Br doping. The influence of Mn doping on the PL of $CsPbCl_3Br_{3-x}$ is also investigated

Introduction

Inorganic nanocrystals including $CsPbCl_3$, $CsPbBr_3$, and $CsPbI_3$ have attracted a lot of attention due to the excellent application potential in lighting and display, light-harvesting, and optoelectronic devices.[1–13] $CsPbCl_3$ nanocrystals with very strong blue emissions and a large bandgap of 3.1 eV are extensively studied.[14–25] Green and red emissions are also necessary for the application of lighting and display.[26] $CsPbBr_3$ and $CsPbI_3$ exhibit green and red emissions due to their bang gaps.[1,27–41] However, low PL quantum yield and poor stability of $CsPbI_3$ limit its application. Doping of active ions in crystal lattices exhibits significant potential in tuning the optical properties. It is reported that Mn ions can be used to dope in $CsPbCl_3$ to control the optical properties,[42–48] where the red emission from Mn^{2+} due to the transitions of $^4T_1 \rightarrow {}^6A_1$ were observed.[49] Mn is almost the only doping ion that can be commonly prepared by the reported methods. However, it is still challenging to prepare other metal doping in $CsPbCl_3$ nanocrystals by the reported methods.

Mn doping has been reported in $CsPbCl_3$ in many papers. It is commonly accepted that Mn can be doped into $CsPbCl_3$ to produce red emissions. However, Mn-doped in $CsPbBr_3$ and $CsPbI_3$ nanocrystals are rarely reported due to the unsuccessful Mn doping in $CsPbBr_3$ and $CsPbI_3$. There is one paper about Mn-doped $CsPbBr_3$, and the exciton emission of $CsPbBr_3$ disappears.[50] Another paper also claimed the Mn doping in $CsPbBr_3$. However, bule emission is reported in their system, not green emission. [51] It is very possible that the lattice parameters of $CsPbBr_3$ are not suitable for Mn doping. Therefore, the doping of Mn in $CsPbBr_3$ is not clear until now. Anion doping in $CsPbCl_3$, $CsPbBr_3$, and $CsPbI_3$ are much easier than cation doping. $CsPbCl_xBr_{3-x}$ and $CsPbBr_yI_{3-y}$ are widely prepared and studied due to the very similar properties of the same main

group of Cl Br and I.[52–56] It is promising that anion doping can be used to help turn the optical properties of Mn-doped in $CsPbCl_3$ by turning the exciton emissions.

In this work, Tb doped $CsPbCl_3$ nanocrystals are prepared by the hot injection method. The green emissions of Tb from the energy level of $^5D_4$ to $^7F_5$ are observed. Tb and Mn codoped $CsPbCl_3$ nanocrystals are also prepared, but the dominant emission is the red emission of Mn. $MnBr_2$ are used to prepare Mn-doped $CsPbCl_xBr_{3-x}$ nanocrystals. Different concentrations of $MnBr_2$ turn the exciton emissions of $CsPbCl_xBr_{3-x}$ from the blue region to the green region. Meanwhile, red Mn emission is also observed. Mn emission can be observed only in $CsPbCl_3$ component in our $CsPbCl_xBr_{3-x}$ nanocrystals, not the $CsPbBr_3$ component.

Experimental

Chemicals and materials

Manganese bromide hydrate 98%, cesium carbonate 99.9%, lead (II) chloride 99.998%, oleic acid 90% (OA) were purchased from Alfa Aesar. 1-octadecene (ODE, 90%) was purchased from ACROS Organics. Hydrocholride acid (HCl) was purchased from Fisher Chemical. Oleylamine (OLA) was purchased from TCI America.

Preparation of doped $CsPbCl_3$ nanocrystals

The method used in this work is based on Pradhan's method.[57]

(a) Preparation of OLA-HCl: 10 mL OLA and 1 mL HCl were loaded in a 25 ml 3-neck round-bottomed flask. The temperature was raised to 80 °C, and the mixture was purged with nitrogen for 1 hour. Then the solution was kept for 2 h at 120 °C under nitrogen. The solution was stored

under a nitrogen atmosphere. The stock solution was heated to 80 °C when it is needed for the next step.

(b) Preparation of Cs-oleate: Cs_2CO_3 (0.5 mmol, 162.5 mg) was loaded in a three-neck flask along with 10 mL ODE and 1 mL OA. The reaction mixture was purged with nitrogen for 1 h and then the temperature was raised to 150 ^oC to form a clear Cs-oleate solution, which was kept at room temperature for use.

(c) Synthesis of Tb (or Mn) doped $CsPbCl_3$ nanocrystals: 0.1 mmol $PbCl_2$ (27.8 mg), certain amount of $TbCl_3.6H_2O$ and $MnCl_2$ (see Table 1 S1-S7), and 5 mL ODE were loaded in a 100 mL three-neck flask. The solution was purged and then kept at 120 °C for 2 h under nitrogen gas. Then 0.5 mL OA and OLA (previously degassed at 120 °C for 2 h) were injected into the reaction flask. The resulting solution was kept at 120 °C for 30 min. Then 0.5 ml OLA-HCl was injected into the reaction flask. The temperature was then increased to 275 ^oC (see Table 1 S1-S7). Afterward, 0.4 ml Cs-oleate was injected into the above solution swiftly. After 1 minute, the heat was removed, and the nanoparticles were cooled down to room temperature in an ice bath.

(d) Synthesis of $MnBr_2$ doped $CsPbCl_3$ nanocrystals: 0.1 mmol of $PbCl_2$ (27.8 mg), certain amount of $MnBr_2$ (see Table 1 S8-S14) and 5 mL ODE were loaded in a 100 mL three-neck flask. A vacuum was applied to the above solution, and then the solution was kept at 120 °C for 2 h under nitrogen gas. Then 0.5 ml OA and OLA (previously degassed at 120 °C for 2 h) were injected into the reaction flask, and then it was kept at 120 °C for 30 mins. Then 0.5 ml OLA-HCl was injected into the reaction flask. The temperature was then increased to 180 °C and 0.4 mL Cs-oleate was injected swiftly. After 1 minute, the heat was removed and the reaction mixture was cooled down to room temperature in an ice bath.

Table 1 shows the sample information in this work.

Sample name	$PbCl_2$:$TbCl_3$:$MnCl_2$
S1	1:0:0
S2	1:0.2:0
S3	1:0.5:0
S4	1:1:0
S5	1:1.5:0
S6	1:2:0
S7	1:1:0.05

Sample name	$PbCl_2$:$MnBr_2$
S8	1:0.05
S9	1:0.2
S10	1:1
S11	1:2
S12	1:3
S13	1:4
S14	1:5

Characterization methods

The morphology of nanocrystals was characterized by a transmission electron microscope (TEM) (JEM-1011, JEOL). The crystallinity and phase of the $CsPbCl_3$ materials were studied by an X-

ray diffraction system (XRD) (MiniFlex 600, Rigaku). PL spectra and Time-resolved PL (TRPL) spectra were obtained with a fluorescence spectrophotometer (FluoroMax, Horiba) with TCSPC accessories under 370 nm light excitation.

Results and discussion

Figures 1 a and b show the TEM images of the $CsPbCl_3$ S1 and S6 nanocrystals, respectively. The sizes of S1 and S6 are 8 and 12 nm, respectively. It can be observed that cube $CsPbCl_3$ nanocrystals are produced by our method. The average size of $CsPbCl_3$ increases a little as the Tb doped into $CsPbCl_3$ nanocrystals. Therefore, doping induces crystal growth toward large sizes.

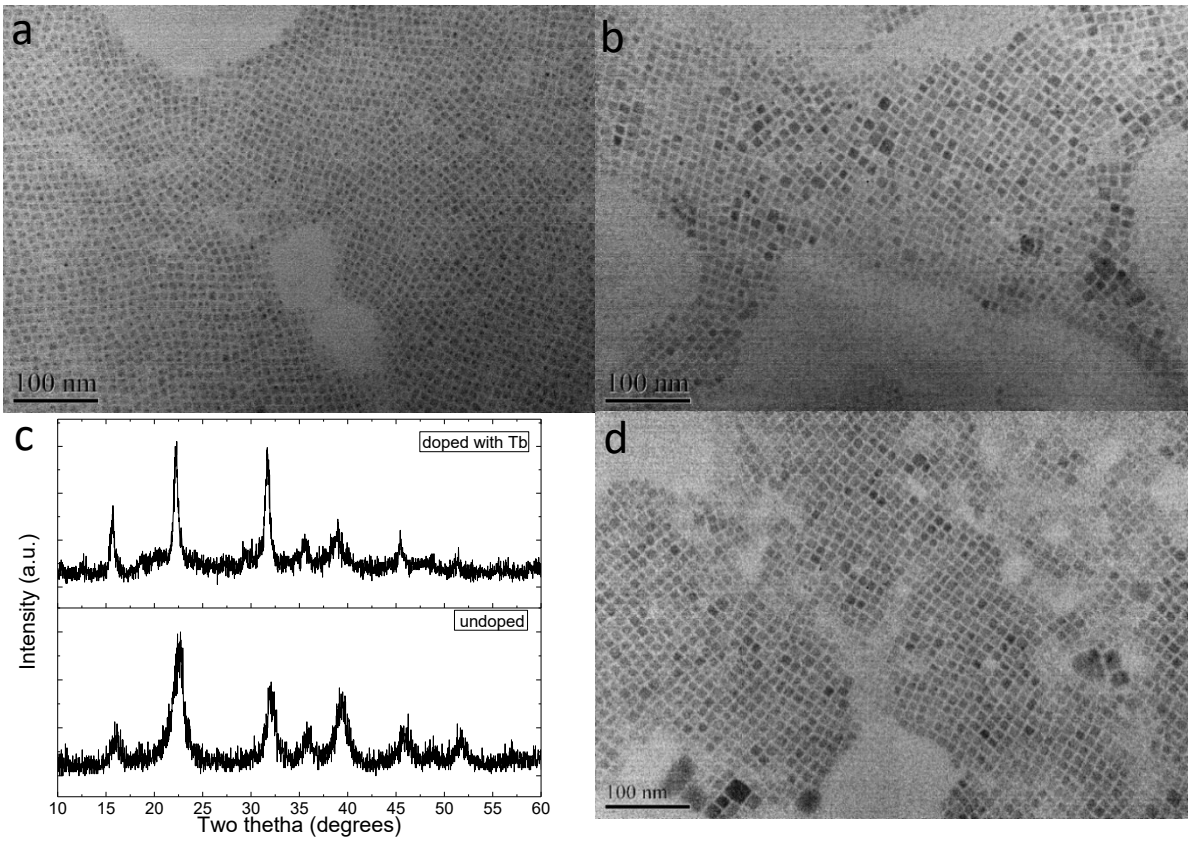

Figure 1 a b TEM images of S1 and S6. c XRD data of S1 and S6. d TEM image of S7.

Figure 1c shows the XRD diffraction patterns of S1 and S6. The diffraction peaks are indexed into tetragonal phase $CsPbCl_3$ structure (JCPDS 18-0366) Tb doping does not affect the crystal structure of $CsPbCl_3$ nanocrystals. The diffraction peaks of S6 are much narrower than that of S1, which is explained by the larger sizes. Based on Scherrer equation, smaller size of NCs can cause the broadening of XRD peaks. Therefore XRD data is consistent with the size of the products from TEM result. Figure 1d shows the TEM image of S7. The average size of the S7 is 12 nm with some large particles in the images. Therefore, Tb doping leads to large particle sizes of $CsPbCl_3$ nanocrystals, but the morphology doesn't change.

Figure 2 a-f shows the photoluminescence (PL) properties of the synthesized $CsPbCl_3$ nanocrystals with different Tb concentrations (λ_{ex}=330 nm). The PL peak at ~400 nm is attributed to $CsPbCl_3$ exciton emission. The peak at ~543 nm is attributed to the transition of $^5D_4 \rightarrow {}^7F_5$ energy levels of Tb^{3+}.[58] It can be observed that the relative peak intensity of peaks at ~543 nm to ~400 nm increases as the Tb concentration increases as the $PbCl_2$:$TbCl_3$ is less than 1:1, indicating Tb doping concentration in $CsPbCl_3$ nanocrystals increases as the ratio of $PbCl_2$:$TbCl_3$ increases. The PL relative peak intensity of peaks at ~543 nm to ~400 nm decreases as the $PbCl_2$:$TbCl_3$ is more than 1:1. The 543 nm PL peak is very weak for S6 (Figure 2f). This is attributed to the Tb PL quench caused by high Tb concentration.[58] Therefore, the optimized Tb PL is obtained as the $PbCl_2$:$TbCl_3$ is 1:1 (figure 2d). Figures 2g and h show the PL excitation (PLE) spectra of Tb doped $CsPbCl_3$ S4 monitored at 400 nm and 543 nm, respectively. Two spectra are very similar to each other. This indicates the energy transfer from $CsPbCl_3$ to Tb. Figure 2i shows the PLE spectrum of undoped $CsPbCl_3$ S1 monitored at 400 nm. Compared to the spectra of the Tb doped $CsPbCl_3$ (figure 2g), It can be seen that the excitation spectrum of $CsPbCl_3$ is modified by Tb doping. However, the PL spectra are not influenced by Tb doping (figure 2a-f). Therefore, Tb doping can

modify the optical properties, leading to the green emission of the nanocrystals. Energy transfer from $CsPbCl_3$ matrix to Tb is identified from the PLE spectra.

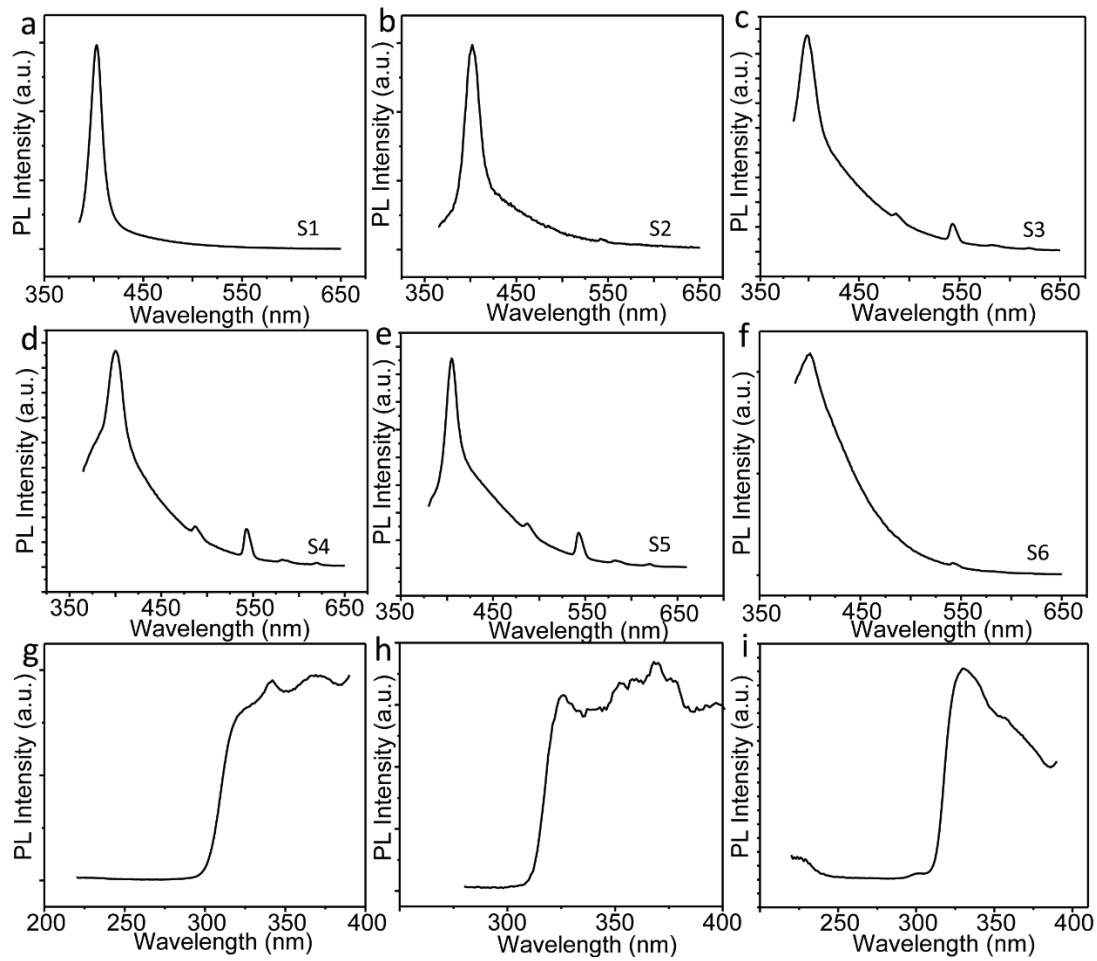

Figure 2 a-f PL spectra of S1-S6 (λ_{ex}=330 nm). g-h PLE spectra λ_{em}=400 nm, λ_{em}=543 nm of S4. i PLE spectra of S1 λ_{em}=400 nm.

Tb and Mn ions are used to co-doped into $CsPbCl_3$ S7 nanocrystals to study the optical properties. Figures 3a, b, and c show the PL spectra under the excitation of 290 nm, 350 nm, and 370 nm, respectively. The exciton PL peak at ~400 nm is exhibited, which confirms the $CsPbCl_3$ production. Broadband at ~ 590 nm is attributed to the emission of Mn^{2+},[49] which indicates the successful Mn doping into the $CsPbCl_3$ crystal lattice. In addition, the tiny peak at 543 nm is

attributed to the Tb^{3+} emission shown in figure 3a, which is consistent with the results in figure 2. Tb emission in Tb, Mn coped $CsPbCl_3$ nanocrystals is very week compared to that of Mn. PLE spectra of S7 are shown in figure 3d-f. It can be observed that all the PLE spectra are in the region of 300 nm-400 nm. PLE spectrum of S7 monitored at 400 nm is similar to that of S4 Tb doped $CsPbCl_3$. A sharp component at ~300 nm and a broad component are observed for Figures 3d and e. The sharp component shows dominated intensity in figure 3e, indicating that the efficient absorption at 300 nm is responsible for Tb emission. While the component at ~400 nm in the PLE spectrum monitored at 590 nm in figure 3f shows that the 400 nm component in the PLE spectrum leads to Mn emission. Therefore, the Tb Mn codoped $CsPbCl_3$ nanocrystals show dominated Mn emission even though the Mn doping concentration is very low compared to that of Tb.

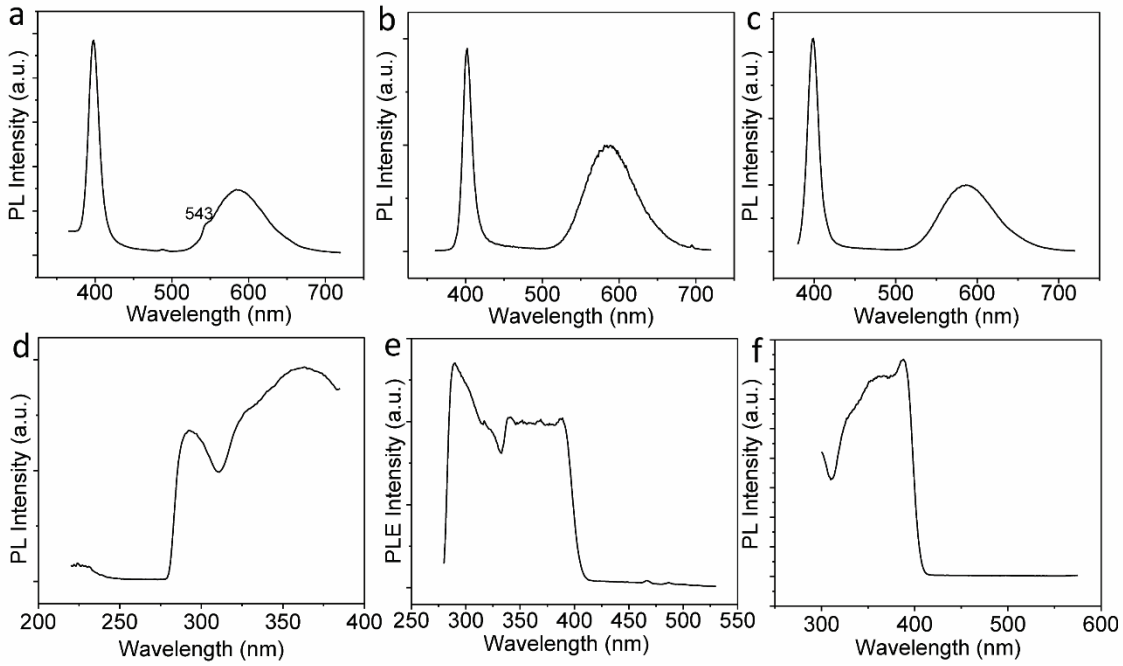

Figure 3 PL spectra of S7 a λ_{ex}=290 nm, b λ_{ex}=350 nm, c λ_{ex}=370 nm. PLE spectra of S7 d λ_{em}=400 nm e λ_{em}=543 nm f λ_{em}=590 nm.

Photodetectors with a device configuration of FTO/TiO_2/$CsPbCl_3$ /Spiro/Au are fabricated. Figures 4 and b show the photodetector performance of the devices based on S1 and S4, respectively. It can be observed that the photocurrent increases with the increasing light density for both devices. The photocurrent of the device based on S4 is much higher than that of the S1, which is explained by the improved crystallinity of Tb doped samples due to large sizes (Figure 1c). Therefore, Tb doping also improves photodetector performance.

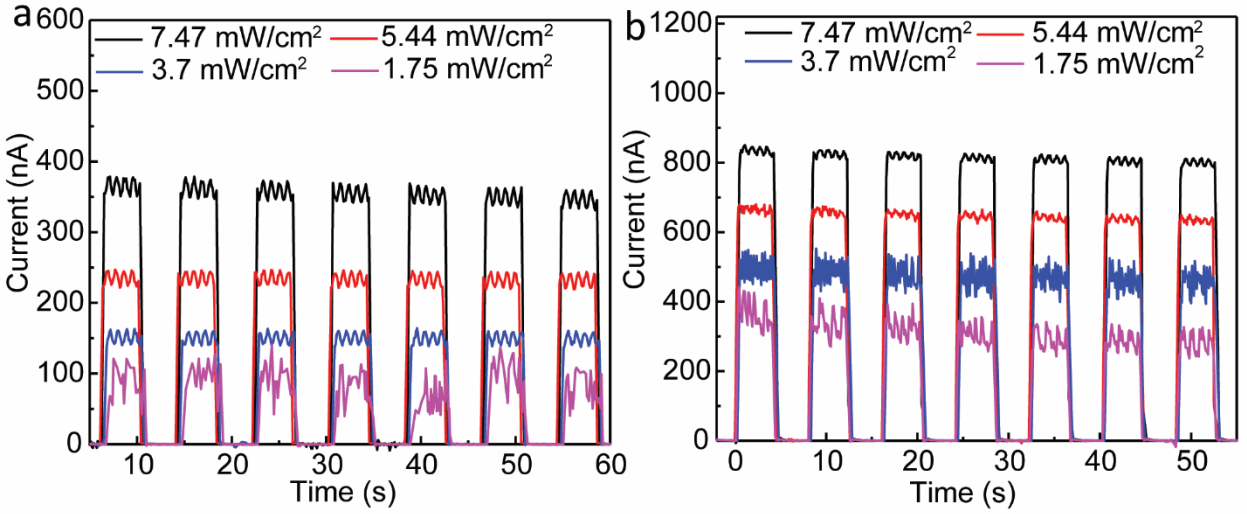

Figure 4 photodetector performance of the devices based on S1 and S4.

$MnBr_2$ is used to prepare Mn-doped $CsPbCl_xBr_{3-x}$ nanocrystals since Mn^{2+} and Br^- will be introduced to $CsPbCl_3$ nanocrystals. Figure 5 shows the TEM images of S8, S9, and S12. The average sizes of $CsPbCl_xBr_{3-x}$ S8, S9, and S12 are 10 nm, 11 nm, and 10 nm, respectively. The average sizes don't change that much. Figure 5d shows the XRD diffraction patterns of S1, S9, and S12. It can be seen that the three samples show the same XRD diffraction patterns, indicating the Mn and Br doping doesn't affect the crystal structure of $CsPbCl_3$.

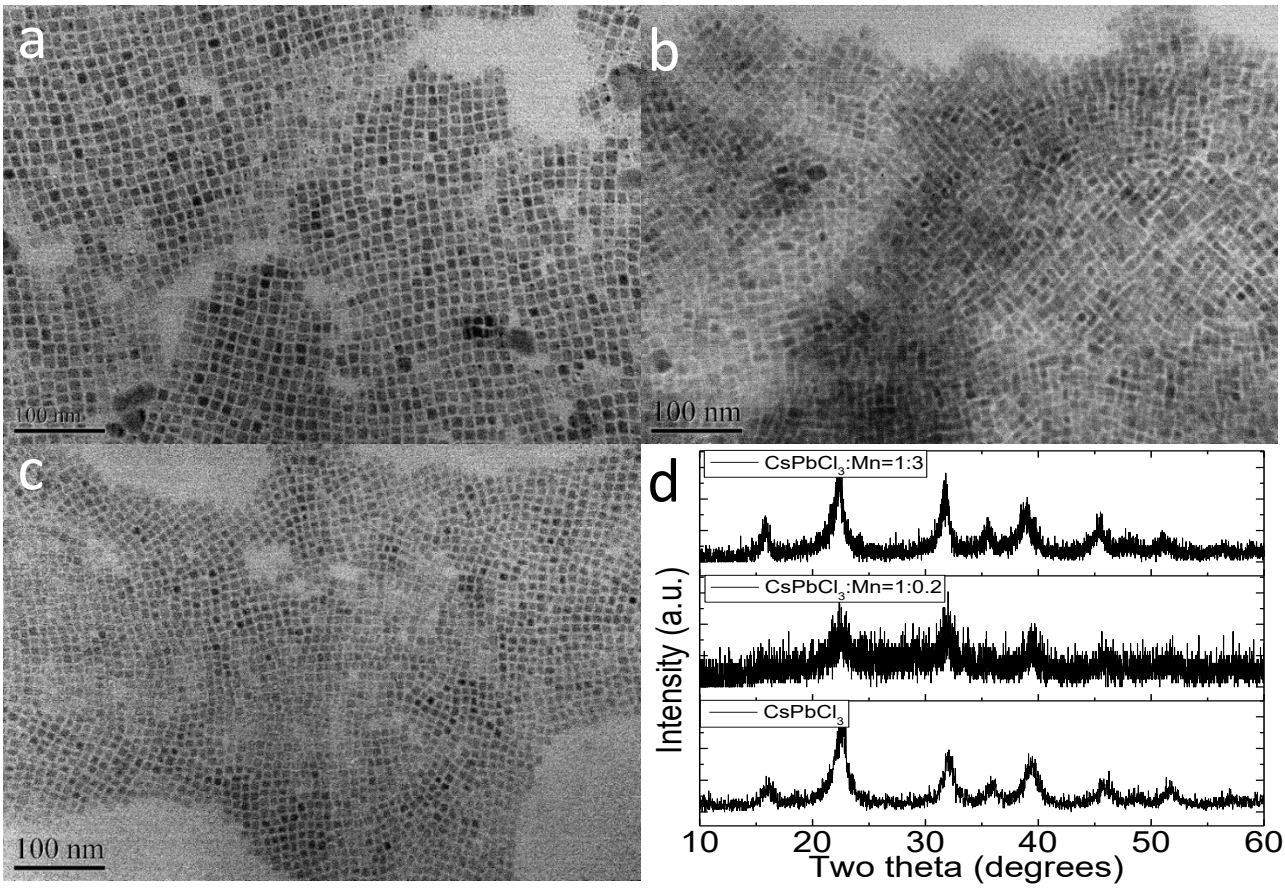

Figure 5 a b c SEM images S8, S9, and S12. d XRD diffractions patterns of S1, S9 and S12.

Figure 6 shows PL spectra of S8-S14. All the spectra in the figure consist of a sharp exciton emission of $CsPbClxBr_{3-x}$ and a broadband emission of Mn^{2+}. The exciton emission peaks are located at 400 nm, 400 nm, 409 nm, 415 nm, 428 nm, 459 nm, and 480 nm for S8, S9, S10, S11, S12, S13, and S14, respectively. It can be seen that the exciton emission peak positions redshift as more Br^- ions are doped into $CsPbCl_3$, which can be explained by the production of $CsPbBr_3$. $CsPbBr_3$ produces green emission with an emission peak at ~500 nm.[1] The introduction of $MnBr_2$ induces the production of the $CsPbBr_3$ component in the $CsPbClxBr_{3-x.}$ More $CsPbBr_3$ components will be produced as more $MnBr_2$ is introduced into the $CsPbCl_3$, leading to the redshift of the exciton emission peak. The relative intensity ratio of Mn emission to the exciton peak from

$CsPbClxBr_{3-x}$ increases as the ratio of $PbCl_2$:$MnBr_2$ increases from 1:0.05 to 1:1 (S8-S10). The relative intensity ratio decreases as the ratio of $PbCl_2$:$MnBr_2$ further increases from 1:2 to 1:5 (S11-S14). It is a challenge to dope Mn in $CsPbBr_3$ based on this method. Mn can be only doped into the $CsPbCl_3$ component by this method. The decreased Mn emission caused by the increased $MnBr_2$ amount is attributed to the decreased amount of $CsPbCl_3$ in the sample, leading to decreased Mn doping in the samples. The Mn emission of S14 almost disappears as the ratio of $PbCl_2$ to $MnBr_2$ is 1:5 (Figure 6g). The exciton emission peak is located at 480 nm. This indicates the $CsPbCl_3$ phase still exists in S14 since the exciton emission peak of $CsPbBr_3$ is located at ~500 nm.[1] The absence of Mn emission in S14 is attributed to the disordered phase of $CsPbCl_3Br_{3-x}$ caused by the Br doping in $CsPbCl_3$. We also try to synthesize Mn-doped $CsPbBr_3$ by this method. However, Mn emission cannot be observed in our samples. Therefore, a certain amount of $CsPbCl_3$ lattice is necessary for Mn doping for our method. Recently reports indicate that the missing of Mn emission in $CsPbBr_3$ due to the low bandgap of $CsPbBr_3$ and back energy transfer from Mn dopants to host.[59] Therefore, it is possible that Mn actually doped in the $CsPbBr_3$ in this study. In addition, it was reported that Mn doping can help increase the PLQY and stability of $CsPbBr_3$ NCs even though no Mn emission was observed.[60] Figures 6 h and i show the photodetector performance of the devices based on S8 and S13. The performance of the device based on S8 is measured under 400 nm light. The performance of the device based on S13 is measured under the 459 nm light. The two devices show similar device performance. Therefore, $MnBr_2$ doping can be used to tune the photodetector working wavelength.

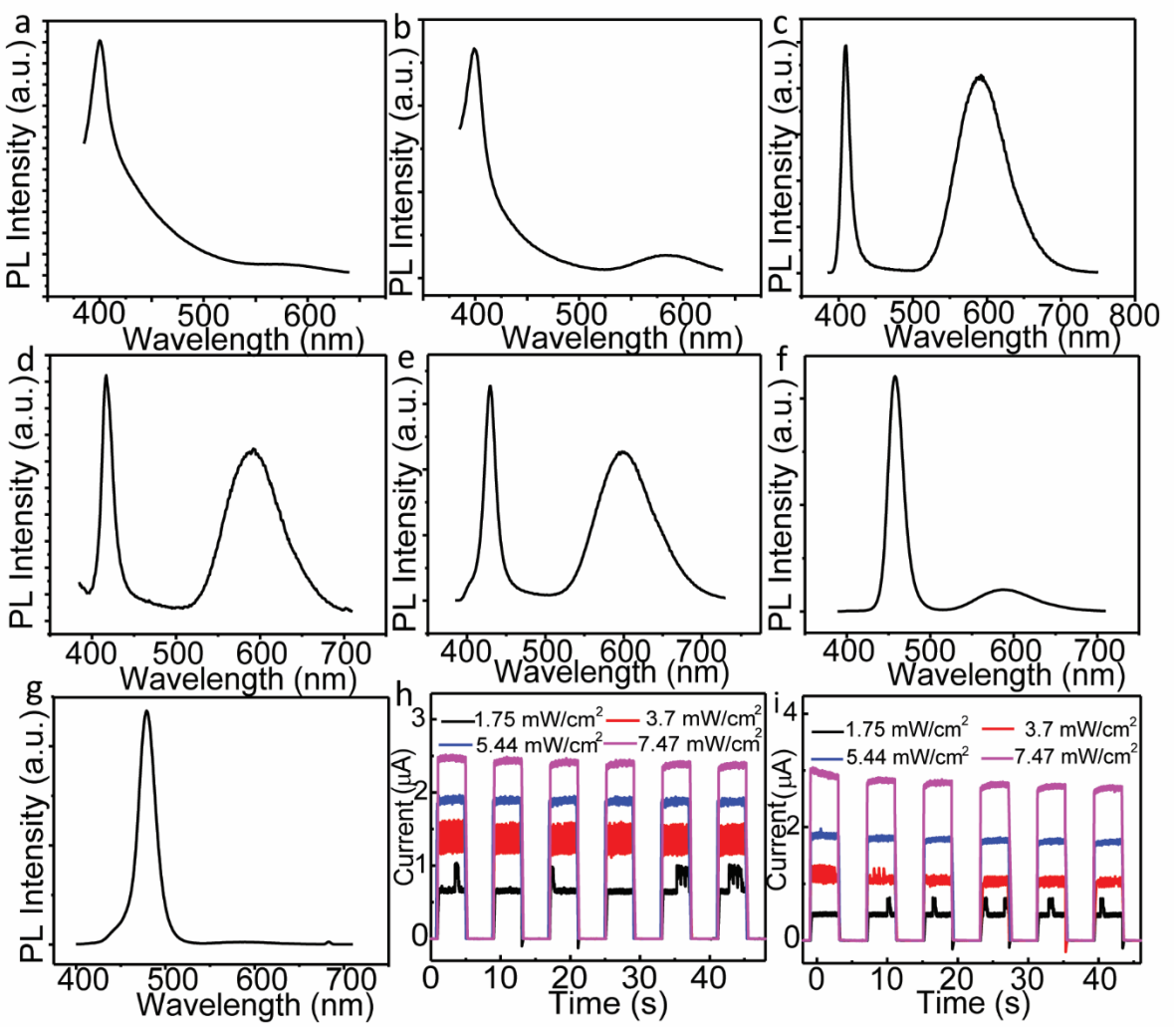

Figure 6 a-g the PL spectra of S8-S14. h and i photodetector performance of the devices based on S8 and S13

Conclusions

$CsPbCl_3$ nanocrystals doped with Tb, Mn, and Br are synthesized by the hot injection method in this work. The characteristic emission peak of Tb^{3+} at 543 nm is observed for $CsPbCl_3$:Tb nanocrystals, and the dominated emission is still from the $CsPbCl_3$ host. The Tb emission intensity decreases as Tb and Mn codoped into $CsPbCl_3$ nanocrystals. The dominated Mn emission is obtained as Tb and Mn are codoped into $CsPbCl_3$ nanocrystals. Mn and Br are also codoped into $CsPbCl_3$ nanocrystals to prepare $CsPbCl_3Br_{3-x}$ nanocrystals. The exciton emission of the

$CsPbCl_3Br_{3-x}$ nanocrystals exhibits redshift due to the introduction of Br in $CsPbCl_3$. This induces the Mn emission intensity to be controlled by the $CsPbCl_3$ crystal lattice. This method controls the emission color of $CsPbCl_3$ nanocrystals.

Declaration of Competing Interest

The authors declare that they have no known competing financial interests or personal relationships that could have appeared to influence the work reported in this paper.

Acknowledgment

This work is supported by NSF-PREM grant #DMR-1826886. The TRPL equipment used in this work is supported by National Science Foundation Research Initiation Award: Novel Perovskite Solar Cells Based on Interface Manipulation (Award#1900047). The XRD used in this work is supported by the U.S. Army Engineer Research and Development Center (W912HZ-16-2-0021).

References

[1] C.H. Kang, I. Dursun, G. Liu, L. Sinatra, X. Sun, M. Kong, J. Pan, P. Maity, E.-N. Ooi, T.K. Ng, O.F. Mohammed, O.M. Bakr, B.S. Ooi, High-speed colour-converting photodetector with all-inorganic CsPbBr 3 perovskite nanocrystals for ultraviolet light communication, Light Sci. Appl. 8 (2019) 94. https://doi.org/10.1038/s41377-019-0204-4.

[2] S. Cho, S. Kim, J. Kim, Y. Jo, I. Ryu, S. Hong, J.-J. Lee, S. Cha, E.B. Nam, S.U. Lee, S.K. Noh, H. Kim, J. Kwak, H. Im, Hybridisation of perovskite nanocrystals with organic molecules for highly efficient liquid scintillators, Light Sci. Appl. 9 (2020) 156. https://doi.org/10.1038/s41377-020-00391-8.

[3] Y. Miao, L. Cheng, W. Zou, L. Gu, J. Zhang, Q. Guo, Q. Peng, M. Xu, Y. He, S. Zhang, Y. Cao, R. Li, N. Wang, W. Huang, J. Wang, Microcavity top-emission perovskite light-emitting diodes, Light Sci. Appl. 9 (2020) 89. https://doi.org/10.1038/s41377-020-0328-6.

[4] X. Li, X. Liu, X. Liu, Self-assembly of colloidal inorganic nanocrystals: nanoscale forces, emergent properties and applications, Chem. Soc. Rev. (2020). https://doi.org/10.1039/D0CS00436G.

[5] M. Liu, N. Yan, C. Zhang, L. Li, Integrated solar cells with non-toxic inorganic nanocrystals and polymer bulk heterojunction, Appl. Surf. Sci. Adv. 3 (2021) 100052. https://doi.org/10.1016/j.apsadv.2020.100052.

[6] J. Li, J. Li, R. Liu, Y. Tu, Y. Li, J. Cheng, T. He, X. Zhu, Autonomous discovery of optically active chiral inorganic perovskite nanocrystals through an intelligent cloud lab, Nat. Commun. 11 (2020) 2046. https://doi.org/10.1038/s41467-020-15728-5.

[7] J.-P. Ma, J.-K. Chen, J. Yin, B.-B. Zhang, Q. Zhao, Y. Kuroiwa, C. Moriyoshi, L. Hu, O.M. Bakr, O.F. Mohammed, H.-T. Sun, Doping Induces Structural Phase Transitions in All-Inorganic Lead Halide Perovskite Nanocrystals, ACS Mater. Lett. 2 (2020) 367–375. https://doi.org/10.1021/acsmaterialslett.0c00059.
[8] T. Wang, Z. Yang, L. Yang, X. Yu, L. Sun, J. Qiu, D. Zhou, W. Lu, S.F. Yu, Y. Lin, X. Xu, Atomic-Scale Insights into the Dynamics of Growth and Degradation of All-Inorganic Perovskite Nanocrystals, J. Phys. Chem. Lett. 11 (2020) 4618–4624. https://doi.org/10.1021/acs.jpclett.0c01220.
[9] J. Kim, L. Hu, H. Chen, X. Guan, P.R. Anandan, F. Li, J. Tang, C.-H. Lin, K. Kalantar-Zadeh, A. Tricoli, T. Wu, P-type Charge Transport and Selective Gas Sensing of All-Inorganic Perovskite Nanocrystals, ACS Mater. Lett. 2 (2020) 1368–1374. https://doi.org/10.1021/acsmaterialslett.0c00346.
[10] A. Granados del Águila, T.T.H. Do, J. Xing, W.J. Jee, J.B. Khurgin, Q. Xiong, Efficient up-conversion photoluminescence in all-inorganic lead halide perovskite nanocrystals, Nano Res. 13 (2020) 1962–1969. https://doi.org/10.1007/s12274-020-2840-7.
[11] G.H. Ahmed, J. Yin, O.M. Bakr, O.F. Mohammed, Near-unity photoluminescence quantum yield in inorganic perovskite nanocrystals by metal-ion doping, J. Chem. Phys. 152 (2020) 020902. https://doi.org/10.1063/1.5131807.
[12] J. Dai, J. Xi, Y. Zu, L. Li, J. Xu, Y. Shi, X. Liu, Q. Fan, J. Zhang, S. Wang, F. Yuan, H. Dong, B. Jiao, X. Hou, Z. Wu, Surface mediated ligands addressing bottleneck of room-temperature synthesized inorganic perovskite nanocrystals toward efficient light-emitting diodes, Nano Energy. 70 (2020) 104467. https://doi.org/10.1016/j.nanoen.2020.104467.
[13] H. Zhao, Z. Hu, L. Wei, P. Zeng, C. Kuang, X. Liu, S. Bai, F. Gao, M. Liu, Efficient and High-Luminance Perovskite Light-Emitting Diodes Based on CsPbBr3 Nanocrystals Synthesized from a Dual-Purpose Organic Lead Source, Small. 16 (2020) 2003939. https://doi.org/10.1002/smll.202003939.
[14] J. Zhang, Q. Wang, X. Zhang, J. Jiang, Z. Gao, Z. Jin, Shengzhong (Frank) Liu, High-performance transparent ultraviolet photodetectors based on inorganic perovskite CsPbCl 3 nanocrystals, RSC Adv. 7 (2017) 36722–36727. https://doi.org/10.1039/C7RA06597C.
[15] M. Baranowski, P. Plochocka, P. Plochocka, R. Su, L. Legrand, T. Barisien, F. Bernardot, Q. Xiong, C. Testelin, M. Chamarro, Exciton binding energy and effective mass of $CsPbCl_3$: a magneto-optical study, Photonics Res. 8 (2020) A50–A55. https://doi.org/10.1364/PRJ.401872.
[16] W. Lv, M. Xu, L. Ge, X. Zhu, J. Hong, W. Huang, R. Chen, Two-phase anion exchange synthesis: multiple passivation for highly efficient and stable CsPbCl3 nanocrystals, J. Mater. Chem. C. 8 (1399) 16083–16091. https://doi.org/10.1039/D0TC03602A.
[17] Z. Rao, Z. Rao, Z. Rao, W. Liang, W. Liang, W. Liang, H. Huang, H. Huang, J. Ge, J. Ge, J. Ge, W. Wang, S. Pan, S. Pan, S. Pan, High sensitivity and rapid response ultraviolet photodetector of a tetragonal $CsPbCl_3$ perovskite single crystal, Opt. Mater. Express. 10 (2020) 1374–1382. https://doi.org/10.1364/OME.388429.
[18] Y. He, C.C. Stoumpos, I. Hadar, Z. Luo, K.M. McCall, Z. Liu, D.Y. Chung, B.W. Wessels, M.G. Kanatzidis, Demonstration of Energy-Resolved γ-Ray Detection at Room Temperature by the CsPbCl3 Perovskite Semiconductor, J. Am. Chem. Soc. (2021). https://doi.org/10.1021/jacs.0c12254.
[19] M.A. Uddin, J.D. Glover, S.M. Park, J.T. Pham, K.R. Graham, Growth of Highly Stable and Luminescent CsPbX3 (X = Cl, Br, and I) Nanoplates via Ligand Mediated Anion Exchange of CsPbCl3 Nanocubes with AlX3, Chem. Mater. 32 (2020) 5217–5225. https://doi.org/10.1021/acs.chemmater.0c01325.
[20] J. Zhu, Y. Zhu, J. Huang, L. Hou, J. Shen, C. Li, Synthesis of monodisperse water-stable surface Pb-rich CsPbCl3 nanocrystals for efficient photocatalytic CO2 reduction, Nanoscale. 12 (2020) 11842–11846. https://doi.org/10.1039/D0NR02917C.

[21] W. Zhu, M. Deng, D. Chen, Z. Zhang, W. Chai, D. Chen, H. Xi, J. Zhang, C. Zhang, Y. Hao, Dual-Phase CsPbCl3–Cs4PbCl6 Perovskite Films for Self-Powered, Visible-Blind UV Photodetectors with Fast Response, ACS Appl. Mater. Interfaces. 12 (2020) 32961–32969. https://doi.org/10.1021/acsami.0c09910.
[22] L.Y. Bai, S.W. Wang, Y.W. Zhang, K.X. Zhang, L.X. Yi, Influence of annealing process on the stable luminous CsPbCl3 perovskite films by thermal evaporation, J. Lumin. 227 (2020) 117592. https://doi.org/10.1016/j.jlumin.2020.117592.
[23] R. Sun, D. Zhou, Y. Wang, W. Xu, N. Ding, L. Zi, X. Zhuang, X. Bai, H. Song, Highly efficient ligand-modified manganese ion doped CsPbCl3 perovskite quantum dots for photon energy conversion in silicon solar cells, Nanoscale. 12 (2020) 18621–18628. https://doi.org/10.1039/D0NR04885B.
[24] M. Naseri, D.M. Hoat, R. Ponce-Pérez, J.F. Rivas-Silva, G.H. Cocoletzi, Examining the uniform strain effect on elastic, electronic and optical properties of CsPbCl3 through FP-LAPW calculations, Chem. Phys. 531 (2020) 110654. https://doi.org/10.1016/j.chemphys.2019.110654.
[25] Z.-J. Li, E. Hofman, A.H. Davis, A. Khammang, J.T. Wright, B. Dzikovski, R.W. Meulenberg, W. Zheng, Complete Dopant Substitution by Spinodal Decomposition in Mn-Doped Two-Dimensional CsPbCl3 Nanoplatelets, Chem. Mater. 30 (2018) 6400–6409. https://doi.org/10.1021/acs.chemmater.8b02657.
[26] Thermal and photo stability of all inorganic lead halide perovskite nanocrystals - Physical Chemistry Chemical Physics (RSC Publishing), (n.d.). https://pubs.rsc.org/en/content/articlelanding/2021/cp/d1cp02119b/unauth (accessed August 17, 2021).
[27] C.-C. Lin, S.-K. Huang, C.-E. Hsu, Y.-C. Huang, C.-Y. Wei, C.-Y. Wen, S.-S. Li, C.-W. Chen, C.-C. Chen, Exploring the Origin of Phase-Transformation Kinetics of CsPbI3 Perovskite Nanocrystals Based on Activation Energy Measurements, J. Phys. Chem. Lett. 11 (2020) 3287–3293. https://doi.org/10.1021/acs.jpclett.0c00443.
[28] Y. Wang, Y. Chen, T. Zhang, X. Wang, Y. Zhao, Chemically Stable Black Phase CsPbI3 Inorganic Perovskites for High-Efficiency Photovoltaics, Adv. Mater. 32 (2020) 2001025. https://doi.org/10.1002/adma.202001025.
[29] S. Mahato, A. Ghorai, S.K. Srivastava, M. Modak, S. Singh, S.K. Ray, Highly Air-Stable Single-Crystalline β-CsPbI3 Nanorods: A Platform for Inverted Perovskite Solar Cells, Adv. Energy Mater. 10 (2020) 2001305. https://doi.org/10.1002/aenm.202001305.
[30] S. Wang, C. Bi, A. Portniagin, J. Yuan, J. Ning, X. Xiao, X. Zhang, Y.Y. Li, S.V. Kershaw, J. Tian, A.L. Rogach, CsPbI3/PbSe Heterostructured Nanocrystals for High-Efficiency Solar Cells, ACS Energy Lett. 5 (2020) 2401–2410. https://doi.org/10.1021/acsenergylett.0c01222.
[31] Y. Wang, G. Chen, D. Ouyang, X. He, C. Li, R. Ma, W.-J. Yin, W.C.H. Choy, High Phase Stability in CsPbI3 Enabled by Pb–I Octahedra Anchors for Efficient Inorganic Perovskite Photovoltaics, Adv. Mater. 32 (2020) 2000186. https://doi.org/10.1002/adma.202000186.
[32] J. Khan, X. Zhang, J. Yuan, Y. Wang, G. Shi, R. Patterson, J. Shi, X. Ling, L. Hu, T. Wu, S. Dai, W. Ma, Tuning the Surface-Passivating Ligand Anchoring Position Enables Phase Robustness in CsPbI3 Perovskite Quantum Dot Solar Cells, ACS Energy Lett. 5 (2020) 3322–3329. https://doi.org/10.1021/acsenergylett.0c01849.
[33] C. Huo, C.F. Fong, M.-R. Amara, Y. Huang, B. Chen, H. Zhang, L. Guo, H. Li, W. Huang, C. Diederichs, Q. Xiong, Optical Spectroscopy of Single Colloidal CsPbBr3 Perovskite Nanoplatelets, Nano Lett. 20 (2020) 3673–3680. https://doi.org/10.1021/acs.nanolett.0c00611.
[34] S. Kumar, M. Regue, M.A. Isaacs, E. Freeman, S. Eslava, All-Inorganic CsPbBr3 Nanocrystals: Gram-Scale Mechanochemical Synthesis and Selective Photocatalytic CO2 Reduction to Methane, ACS Appl. Energy Mater. 3 (2020) 4509–4522. https://doi.org/10.1021/acsaem.0c00195.

[35] H.M. Ghaithan, Z.A. Alahmed, S.M.H. Qaid, M. Hezam, A.S. Aldwayyan, Density Functional Study of Cubic, Tetragonal, and Orthorhombic CsPbBr3 Perovskite, ACS Omega. 5 (2020) 7468–7480. https://doi.org/10.1021/acsomega.0c00197.
[36] K. Shen, H. Xu, X. Li, J. Guo, S. Sathasivam, M. Wang, A. Ren, K.L. Choy, I.P. Parkin, Z. Guo, J. Wu, Flexible and Self-Powered Photodetector Arrays Based on All-Inorganic CsPbBr3 Quantum Dots, Adv. Mater. 32 (2020) 2000004. https://doi.org/10.1002/adma.202000004.
[37] D. Vila-Liarte, M.W. Feil, A. Manzi, J.L. Garcia-Pomar, H. Huang, M. Döblinger, L.M. Liz-Marzán, J. Feldmann, L. Polavarapu, A. Mihi, Templated-Assembly of CsPbBr3 Perovskite Nanocrystals into 2D Photonic Supercrystals with Amplified Spontaneous Emission, Angew. Chem. Int. Ed. 59 (2020) 17750–17756. https://doi.org/10.1002/anie.202006152.
[38] J. Shamsi, D. Kubicki, M. Anaya, Y. Liu, K. Ji, K. Frohna, C.P. Grey, R.H. Friend, S.D. Stranks, Stable Hexylphosphonate-Capped Blue-Emitting Quantum-Confined CsPbBr3 Nanoplatelets, ACS Energy Lett. 5 (2020) 1900–1907. https://doi.org/10.1021/acsenergylett.0c00935.
[39] X. Zhang, Y. Qian, X. Ling, Y. Wang, Y. Zhang, J. Shi, Y. Shi, J. Yuan, W. Ma, α-CsPbBr3 Perovskite Quantum Dots for Application in Semitransparent Photovoltaics, ACS Appl. Mater. Interfaces. 12 (2020) 27307–27315. https://doi.org/10.1021/acsami.0c07667.
[40] Y. Chen, S.R. Smock, A.H. Flintgruber, F.A. Perras, R.L. Brutchey, A.J. Rossini, Surface Termination of CsPbBr3 Perovskite Quantum Dots Determined by Solid-State NMR Spectroscopy, J. Am. Chem. Soc. 142 (2020) 6117–6127. https://doi.org/10.1021/jacs.9b13396.
[41] H. Wang, P. Zhang, Z. Zang, High performance CsPbBr3 quantum dots photodetectors by using zinc oxide nanorods arrays as an electron-transport layer, Appl. Phys. Lett. 116 (2020) 162103. https://doi.org/10.1063/5.0005464.
[42] W. Wang, J. Li, G. Duan, H. Zhou, Y. Lu, T. Yan, B. Cao, Z. Liu, Study on the Mn-doped CsPbCl3 perovskite nanocrystals with controllable dual-color emission via energy transfer, J. Alloys Compd. 821 (2020) 153568. https://doi.org/10.1016/j.jallcom.2019.153568.
[43] J. Ghosh, M. Hossain, P.K. Giri, Origin and tunability of dual color emission in highly stable Mn doped CsPbCl3 nanocrystals grown by a solid-state process, J. Colloid Interface Sci. 564 (2020) 357–370. https://doi.org/10.1016/j.jcis.2019.12.066.
[44] F. Sui, M. Pan, Z. Wang, M. Chen, W. Li, Y. Shao, W. Li, C. Yang, Quantum yield enhancement of Mn-doped CsPbCl3 perovskite nanocrystals as luminescent down-shifting layer for CIGS solar cells, Sol. Energy. 206 (2020) 473–478. https://doi.org/10.1016/j.solener.2020.05.070.
[45] Y. Zhao, X. Zhang, C. Xie, W. Shi, P. Yang, S.P. Jiang, Controlling Mn Emission in CsPbCl3 Nanocrystals via Ion Exchange toward Enhanced and Tunable White Photoluminescence, J. Phys. Chem. C. 124 (2020) 27032–27039. https://doi.org/10.1021/acs.jpcc.0c08378.
[46] Z. Cao, J. Li, L. Wang, K. Xing, X. Yuan, J. Zhao, X. Gao, H. Li, Enhancing luminescence of intrinsic and Mn doped CsPbCl3 perovskite nanocrystals through Co2+ doping, Mater. Res. Bull. 121 (2020) 110608. https://doi.org/10.1016/j.materresbull.2019.110608.
[47] J. Yang, X. Yuan, L. Fan, Y. Zheng, F. Ma, H. Li, J. Zhao, H. Liu, Enhancing Mn Emission of CsPbCl3 Perovskite Nanocrystals via Incorporation of Rubidium Ions, Mater. Res. Bull. 133 (2021) 111080. https://doi.org/10.1016/j.materresbull.2020.111080.
[48] D. Zhou, L. Tao, Z. Yu, J. Jiao, W. Xu, Efficient chromium ion passivated CsPbCl3:Mn perovskite quantum dots for photon energy conversion in perovskite solar cells, J. Mater. Chem. C. 8 (2020) 12323–12329. https://doi.org/10.1039/D0TC03115A.
[49] S. Lin, H. Lin, C. Ma, Y. Cheng, S. Ye, F. Lin, R. Li, J. Xu, Y. Wang, High-security-level multi-dimensional optical storage medium: nanostructured glass embedded with LiGa 5 O 8 : Mn 2+ with photostimulated luminescence, Light Sci. Appl. 9 (2020) 22. https://doi.org/10.1038/s41377-020-0258-3.

[50] D. Parobek, Y. Dong, T. Qiao, D.H. Son, Direct Hot-Injection Synthesis of Mn-Doped CsPbBr3 Nanocrystals, Chem. Mater. 30 (2018) 2939–2944. https://doi.org/10.1021/acs.chemmater.8b00310.
[51] Reversible Color Switching in Dual-Emitting Mn(II)-Doped CsPbBr3 Perovskite Nanorods: Dilution versus Evaporation | ACS Energy Letters, (n.d.). https://pubs.acs.org/doi/10.1021/acsenergylett.9b01702 (accessed January 30, 2021).
[52] G. Pan, X. Bai, W. Xu, X. Chen, Y. Zhai, J. Zhu, H. Shao, N. Ding, L. Xu, B. Dong, Y. Mao, H. Song, Bright Blue Light Emission of Ni2+ Ion-Doped CsPbClxBr3–x Perovskite Quantum Dots Enabling Efficient Light-Emitting Devices, ACS Appl. Mater. Interfaces. 12 (2020) 14195–14202. https://doi.org/10.1021/acsami.0c01074.
[53] Q. He, Y. Zhang, Y. Yu, Y. Chen, M. Jin, E. Mei, X. Liang, L. Zhai, W. Xiang, Ultrastable Gd3+ doped CsPbBrI2 nanocrystals red glass for high efficiency WLEDs, Chem. Eng. J. 411 (2021) 128530. https://doi.org/10.1016/j.cej.2021.128530.
[54] L. Yan, M. Wang, C. Zhai, L. Zhao, S. Lin, Symmetry Breaking Induced Anisotropic Carrier Transport and Remarkable Thermoelectric Performance in Mixed Halide Perovskites CsPb(I1–xBrx)3, ACS Appl. Mater. Interfaces. 12 (2020) 40453–40464. https://doi.org/10.1021/acsami.0c07501.
[55] A.S. Jbara, J. Munir, B.U. Haq, M.A. Saeed, Density functional theory study of mixed halide influence on structures and optoelectronic attributes of $CsPb(I/Br)_3$, Appl. Opt. 59 (2020) 3751–3759. https://doi.org/10.1364/AO.389100.
[56] Z. Guo, A.K. Jena, I. Takei, G.M. Kim, M.A. Kamarudin, Y. Sanehira, A. Ishii, Y. Numata, S. Hayase, T. Miyasaka, VOC Over 1.4 V for Amorphous Tin-Oxide-Based Dopant-Free CsPbI2Br Perovskite Solar Cells, J. Am. Chem. Soc. 142 (2020) 9725–9734. https://doi.org/10.1021/jacs.0c02227.
[57] S. Das Adhikari, S.K. Dutta, A. Dutta, A.K. Guria, N. Pradhan, Chemically Tailoring the Dopant Emission in Manganese-Doped CsPbCl3 Perovskite Nanocrystals, Angew. Chem. Int. Ed. 56 (2017) 8746–8750. https://doi.org/10.1002/anie.201703863.
[58] C.C. Lin, W.-T. Chen, C.-I. Chu, K.-W. Huang, C.-W. Yeh, B.-M. Cheng, R.-S. Liu, UV/VUV switch-driven color-reversal effect for Tb-activated phosphors, Light Sci. Appl. 5 (2016) e16066–e16066. https://doi.org/10.1038/lsa.2016.66.
[59] A.H. Davis, W. Zheng, Discrete composition control of two-dimensional morphologic all-inorganic metal halide perovskite nanocrystals, J. Energy Chem. 59 (2021) 257–275. https://doi.org/10.1016/j.jechem.2020.10.023.
[60] S. Zou, Y. Liu, J. Li, C. Liu, R. Feng, F. Jiang, Y. Li, J. Song, H. Zeng, M. Hong, X. Chen, Stabilizing Cesium Lead Halide Perovskite Lattice through Mn(II) Substitution for Air-Stable Light-Emitting Diodes, J. Am. Chem. Soc. 139 (2017) 11443–11450. https://doi.org/10.1021/jacs.7b04000.